11th International Symposium on Magnetic Bearings
August 26-29, Nara, Japan

APPLICATION OF ACTIVE MAGNETIC BEARING FOR TUBULAR LINEAR INDUCTION MOTOR IN OIL PUMPING

Eduardo Alves da Costa
Lab. of Automation and Control, University of São Paulo, São Paulo, 05508-900, Brazil
eduardo.costa@poli.usp.br

Ivan Eduardo Chabu
Lab. of Applied Electromagnetism, University of São Paulo, São Paulo, 05508-900, Brazil
ichabu@pea.usp.br

Jose Jaime da Cruz
Lab. of Automation and Control, University of São Paulo, São Paulo, 05508-900, Brazil
jaime@lac.usp.br

ABSTRACT

An active magnetic bearing (AMB)* to support the shaft of a tubular linear induction motor (TLIM) applied to oil pumping is proposed. Instead of the usual eight-pole AMB, a different concept is adopted where a DC-excited primitive bearingless machine is used as a magnetic bearing. The AMB is a 3-phase one for which a lower number of wires connections and power devices are among its advantages. This paper focuses on the design of the AMB system. A finite element analysis of the flux density and of the relationship between the radial force and the suspension winding current are explored. The magnetic system is modeled and simulation is performed to tune the controller parameters.

Index Terms – Active magnetic bearing, linear induction motor, bearingless motor, feedback control system.

INTRODUCTION

The tubular linear induction motor (TLIM), built by the Applied Electromagnetism Laboratory (LMAG) of the University of São Paulo, Brazil, is a prototype intended to drive a sucker-rod pump system for subterranean oil extraction. This kind of application using a TLIM is new and the motor may replace the mechanical surface system and the rod string with advantages [1]-[3].

In the sucker-rod pump system problems with the flexible parts and rupture of the rod, taking to long stops for maintenance, occur frequently. The use of the equipment can be limited depending on the depth of the oil well. In the TLIM based system, the motor is located at the well bottom directly coupled to the suction pump, thus eliminating the need for the surface sucker-rod system and rod string. A simpler system requiring less maintenance and, consequently, lower costs of production, results. Another important characteristic of this tubular motor is its modular construction that allows adaptation to wells of different depths, by just connecting the appropriate number of modules.

With the increasingly developing technology, Active Magnetic Bearing (AMB) systems have been applied in the last years to various machines such as vacuum pumps, centrifuges, blood pumps, energy storage flywheels and semiconductor processes [4]-[6]. Thus the AMB arises as an interesting alternative to support the shaft (secondary of TLIM) in view of numerous advantages over conventional bearings such as no contact, lower losses caused by axial motion, elimination of the lubrication, active vibration control, longer life and less maintenance.

Instead of the most popular AMB [5] with eight magnetic poles, a different concept [6] is adopted in this project: a DC-excited primitive bearingless (self-bearing) machine. In this kind of magnetic bearing a DC current is used to excite the motor windings and generate a static 4-pole flux distribution that acts as the bias flux, as in the conventional radial magnetic bearing; the 3-phase windings with a 3-phase inverter is used as a suspension winding. Lower numbers of connection wires and power devices are among the advantages of this choice.

Besides the difficulties to control the AMB system, in this case two additional problems arise, namely, the secondary of the TLIM is not homogeneous (ring cage type with carbon steel teeth and copper slots) and it exhibits an axial motion.

* This work is partially supported by FAPESP under grant No. 2008/01900-7.

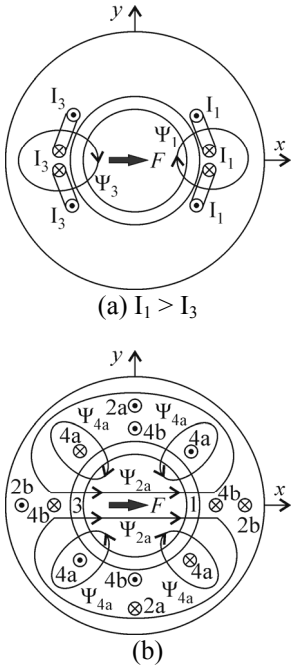

FIGURE 1: *x*-axis direction force: (a) traditional radial magnetic bearing; (b) DC-excited primitive bearingless motor.

This paper focuses on the design of the magnetic bearing system. A finite element analysis of the flux density and of the relationship between the radial force and the suspension winding current are explored. The magnetic system is modeled and simulation with MATLAB is performed to tune the controller parameters.

PRINCIPLE OF RADIAL FORCE GENERATION

A typical 8-pole radial magnetic bearing with radial force generation in the *x*-axis is shown in figure 1a. The eight poles are divided into four electromagnets but only windings 1 and 3 are shown. Denoting the current on winding *i* by I_i then if $I_1 > I_3$ the magnets generate a resultant radial force (F) in *x*-axis direction. The AMB model can be linearized with magnets operating in differential driving mode using bias current. In total, eight wires are necessary for connection between the radial magnetic bearing and the four current drives.

Figure 1b shows the cross section of a DC-excited primitive bearingless machine in the condition that the resultant radial force (F) in the *x*-axis direction is generated supposed that the currents are set to zero in both 2*b* and 4*b* windings. Two sets of windings are wound in the stator. One is a 4-pole torque winding (4*a*) and the other one is a 2-pole radial force winding (2*a*). In this project the bearingless machine does not have the function of torque generation being the DC current used just to excite the torque winding. When the shaft is centered with respect to the stator and there is no current in the suspension winding, a symmetrical 4-pole flux Ψ_{4a} will be produced and the flux density at each airgap will be the same. If a disturbance displacement the shaft occurs towards the negative direction of *x*-axis, the symmetrical flux distribution in the shaft airgap will be broken. In order to bring the shaft back to the central position the current in suspension winding must be controlled. If the coil 2*a* carries a positive current as shown in figure 1b, a 2-pole flux wave Ψ_{2a} is generated. Then, flux density in airgap 1 is increased whereas the flux density in airgap 3 is decreased. Thus, a positive radial force F is produced in order to draw the shaft back to the center. A radial force in the negative direction of *x*-axis can be generated with a negative current in 2*a* wires. Similarly, the radial forces in *y*-axis can be produced by controlling the current of windings 2*b*. Consequently, a radial force is generated by the interaction of the 4-pole static magnetic field and suspension winding currents.

Although for the sake of simplicity just 2-phase windings are described, in this work a 3-phase radial magnetic bearing is under construction.

RADIAL FORCE AND CURRENT RELATIONSHIPS

The following assumptions are made: the magneto-motive force (MMF) can be well approximated by its first harmonic, the magnetic circuit is linear, iron permeability is infinite and eccentric rotor displacement is small with respect to the airgap length. The inductance matrix L of the bearingless motor shown in figure 2b can then be written as [6]

$$\begin{bmatrix} \lambda_{4a} \\ \lambda_{4b} \\ \lambda_{2a} \\ \lambda_{2b} \end{bmatrix} = \underbrace{\begin{bmatrix} L_4 & 0 & M'x & -M'y \\ 0 & L_4 & M'y & M'x \\ M'x & M'y & L_2 & 0 \\ -M'y & M'x & 0 & L_2 \end{bmatrix}}_{L} \underbrace{\begin{bmatrix} i_{4a} \\ i_{4b} \\ i_{2a} \\ i_{2b} \end{bmatrix}}_{I}, \quad (1)$$

where the flux linkages of windings 4*a*, 4*b*, 2*a* and 2*b* are λ_{4a}, λ_{4b}, λ_{2a} and λ_{2b}, respectively; the instantaneous currents of windings 4*a*, 4*b*, 2*a* and 2*b* are i_{4a}, i_{4b}, i_{2a} and i_{2b}, respectively; L_4 and L_2 are self-inductances; M' is the derivative of mutual inductance with respect to the shaft radial displacement x and y, that represents the coupling between the 4-pole and the 2-pole windings. M' can be estimated by:

$$M' = \frac{\pi \mu_0 R l N_2 N_4}{8 g_0^2}, \quad (2)$$

where μ_0 is the permeability of free space, R is the rotor radius, l is the axial length, N_2 is the number of turns of

the 2-pole winding, N_4 is the number of turns of the 4-pole winding and g_0 is the nominal airgap length.

The value of M' can also be obtained by using measurement techniques [6].

Suspension Force

In the linear magnetic circuit the magnetic energy stored in the windings can be written as

$$W_m = \frac{1}{2}[I]^T [L][I]. \quad (3)$$

Defining that suspension forces in x and y directions as F_x and F_y, respectively, the suspension forces are obtained by evaluating the partial derivatives of the magnetic energy with respect to the corresponding radial displacement as

$$\begin{bmatrix} F_x \\ F_y \end{bmatrix} = \begin{bmatrix} \frac{\partial W_m}{\partial x} \\ \frac{\partial W_m}{\partial y} \end{bmatrix} M' \begin{bmatrix} i_{4a} & i_{4b} \\ i_{4b} & -i_{4a} \end{bmatrix} \begin{bmatrix} i_{2a} \\ i_{2b} \end{bmatrix}. \quad (4)$$

In this project the primitive bearingless motor is used only as a radial magnetic bearing. Consequently a DC current of value I_4 excites the motor winding i_{4a} and i_{4b} is set as zero. The equation (4) can be simplified to

$$\begin{bmatrix} F_x \\ F_y \end{bmatrix} = M' I_4 \begin{bmatrix} i_{2a} \\ -i_{2b} \end{bmatrix}. \quad (5)$$

The current I_4 generates only a static magnetic field and is similar to a bias current of a traditional AMB.

SYSTEM CONFIGURATION

The TLIM has a modular construction which allows the adjustment of its total thrust to the force required to lift the oil column from the bottom of the well to the ground surface. A sketch of the cross section of an 1-module TLIM with AMB is shown in figure 2.

The secondary of the TLIM levitates under the action of two radial electromagnetic bearings. Furthermore there are retainer bearings to prevent the secondary from touching down the primary when the AMBs fail to work during operation. They also protect the secondary when dynamic loads exceed the AMB load-carrying capacity.

Active Magnetic Bearing

The radial bearing is fixed to the primary of the motor. This bearing is a DC-excited primitive bearingless 3-phase machine with two sets of windings. The values of the main parameters of both the AMB and the TLIM are listed in table 1.

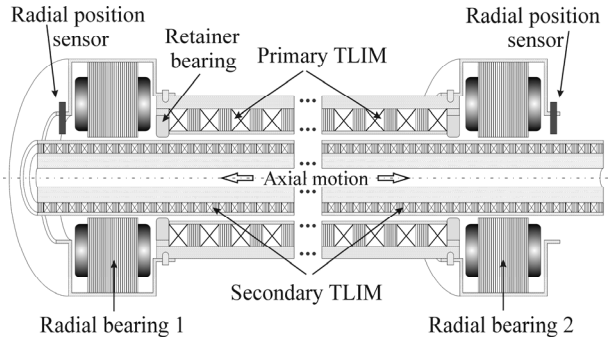

FIGURE 2: Cross section of TLIM with magnetic bearings.

Position sensor

The secondary radial displacement is measured by sensors which have the sensitive element located on the stator x- and y-axes of each magnetic bearing. The secondary of the TLIM is the actuator element. At first glance this seems to be a problem because the secondary is not homogeneous - it has a sort of ring cage with carbon steel teeth and copper slots and the secondary slots are covered by a 1.1mm thick carbon steel plate. Thus an inductive proximity sensor was chosen instead of an eddy current one. The experiments with the TLIM subject to an axial motion showed that the sensor exhibits a linear response not affected by any disturbance due to the non-homogeneous secondary. The sensor has a sensitivity of 2.5mV/μm, a resolution of 1μm and a switching frequency of 1.6kHz.

TABLE 1: Parameters of both the TLIM and the AMB.

Tubular linear induction motor	
Stator outer diameter	124 mm
Length (one module)	750 mm
Synchronous Velocity	1.5 m/s
Secondary outer diameter (shaft)	60.1 mm
Secondary length	2400 mm
Airgap length	1.75 mm
Secondary (shaft) weight	46 kg
Radial active magnetic bearing	
Inner / Outer diameter of the stator	62.5 / 170 mm
Radial airgap length	1.2 mm
Axial length	140 mm
Phases	3

Controller

Figure 3 shows a block diagram of the radial position control system in closed-loop operation. This diagram shows only one magnetic bearing with position and current control. The x- and y-axes radial displacements are compared with reference values x^* and y^*, respectively, which are typically zero. Based on these

errors the position controller evaluates force signals F_x^* and F_y^* to be applied to the secondary. A radial force-current conversion model (which can be equation (5) or an experimental one), is then applied in order to obtain the 2-phase currents commands i_a^* and i_b^*. The three-phase current commands $i_{2u}^*, i_{2v}^*, i_{2w}^*$ are generated employing the inverse Clark coordinate transformation.

The actual current of each phase i_{2u}, i_{2v}, i_{2w} measured from of the power amplifier, is compared to the reference values $i_{2u}^*, i_{2v}^*, i_{2w}^*$ and error is used in the current controller and in the PWM system to generate the control signals for the switches H_A, L_A, H_B, L_B, H_C and L_C of the power devices.

The torque windings are driven by a DC current I_4 that generates a static 4-pole flux distribution or bias flux.

The control system hardware consists of a CompactRIO system with digital and analog input and output modules and of a Field Point Programmable Array (FPGA) to carry out the real-time digital control with high performance. The hardware is complemented by a control application developed in LabVIEW graphical language.

Power Amplifier

The power amplifier used in this project is a one-chip of 3-phase intelligent switching amplifier SA305 from Apex Microtechnology Corporation with three independent half bridge which can provide up to 5A DC. The power amplifier receives the PWM signals generated by the digital control system and sends an analog voltage with information of current for each phase. This power amplifier is a sort of controlled constant-current source that drives the inductive reactance. The PWM frequency range extends to 300KHz.

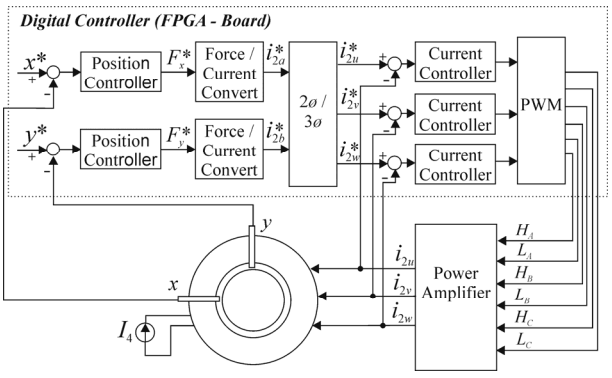

FIGURE 3: System block diagram for closed-loop operation.

TABLE 2: Specifications.

Item	Value
Radial force TLIM	1230 N/mm
Secondary (shaft) weight	46 kg
Saturation flux density	1.2 T
Current density	4.5 A/mm^2
I_4	< 5.5 A
(i_{2a}, i_{2b}) continuous	< 3.0 A

AMB ACTUATOR PROJECT

In accordance with the principle of bearingless motor [6] the numbers of poles of the torque windings and of the control winding must differ by two. This means that the windings must be at least 2- and 4-pole ones. Hence in the 3-phase system the minimum number of stator teeth must be 12, which is the number of slots used in this project. Figure 4 shows both the 4-pole (4u, 4v, 4w) and 2-pole (2u, 2v, 2w) winding sets arrangements.

Considering the specifications of table 2 and performing a finite element analysis (FEA), the AMB actuator was designed. Simulation has been conducted based on the drawing of a model with the magnetic flux density and on the relationship between the radial force and the suspension winding current.

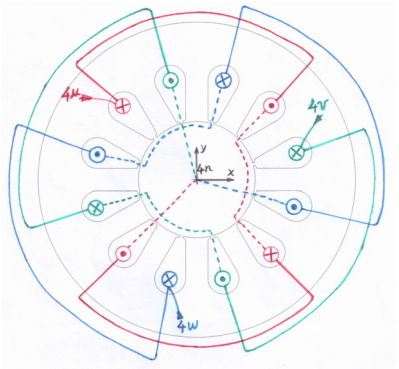

(a) 4-pole winding

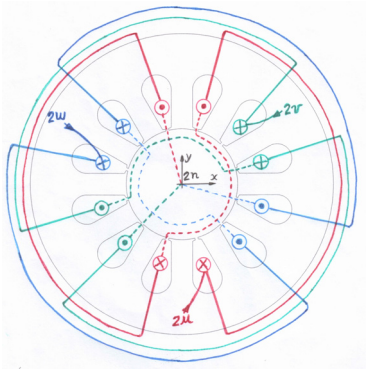

(b) 2- pole winding

FIGURE 4: Winding sets arrangement with 3-phase.

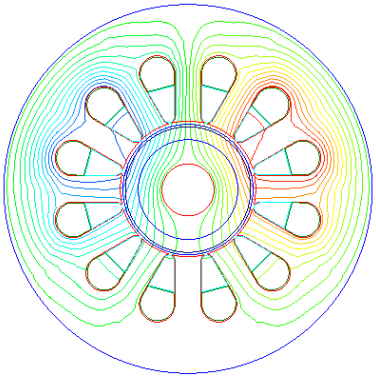

(a) Flux lines

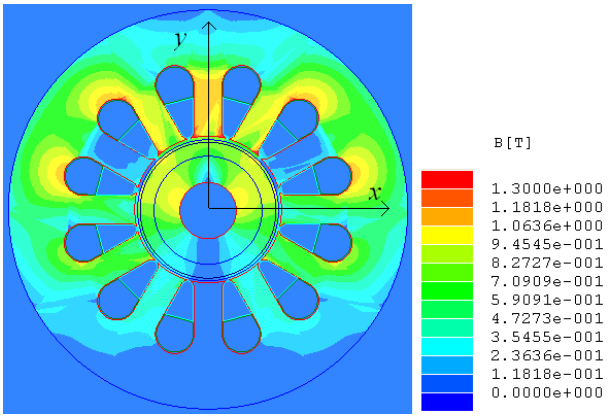

(b) Magnetic flux density distribution

FIGURE 5: FEA simulation of AMB actuator.

Figure 5 is a cross-sectional view of the magnetic bearing showing the flux lines and the magnetic flux density. The worst situation of operation is considered, namely, the secondary of the motor is initially 0.3mm (25% of the airgap) out of the equilibrium position in the negative y-axis with the TLIM in operation. A radial force in the direction of positive y is generated by the magnetic bearing in order to draw the shaft back to center. This force compensates weight of half motor secondary (225N) and of half attraction radial force of the TLIM (185N) with i_{2b}=2.9A and I_4=5.0A.

From figure 5b it can be observed that the magnetic bearing operated out of saturated region where the relationship between radial force and current is linear. Magnetic flux density is smaller than 1.2T.

When the axial length of AMB actuator was defined, care was taken to choose its value as a multiple value of the slot pitch of the secondary motor.

Figure 6 shows the relationships between the suspension current and the radial force obtained by FEA at the condition of nominal airgap. The 4-pole windings were excited by constant DC current I_4 for varying 2-pole currents (i_{2a} or i_{2b}). The radial force obtained was compared to the theoretical values given by equation(5). It can be seen that the theoretical values agree nicely with the FEA values for low values of the exciting current I_4. Nevertheless, during system operation a value of current I_4 between 3A and 5A is considered. In this range the force and current have a good linearity until i_{2b}=4A and the radial force value is greater than the one with I4=1A.

Considering equation (2) and the FEA, the computed values of the derivatives of the mutual inductance M' for both are 34.6H/m and 38.4H/m, respectively.

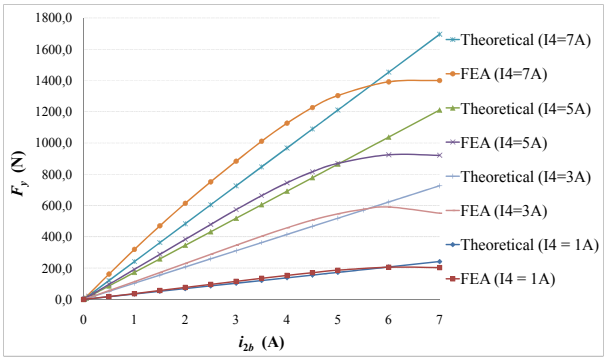

FIGURE 6: Radial force and 2-pole current.

SIMULATION

Figure 7 shows the forces acting on the shaft by two radial magnetic bearings.

The following equations can be written:

$$\begin{cases} m\ddot{x}_1 = F_{x1} + F_{mx1} + d_{x1} \\ m\ddot{y}_1 = F_{y1} + F_{my1} + d_{y1} - mg_a \\ m\ddot{x}_2 = F_{x2} + F_{mx2} + d_{x2} \\ m\ddot{y}_2 = F_{y2} + F_{my2} + d_{y2} - mg_a \end{cases} \quad (6)$$

where m is the mass of half secondary of the motor; g_a is the gravity acceleration; F_{x1} and F_{y1} are the components of the radial force generated by the magnetic bearing 1 along x_1 and y_1-axis directions; F_{x2} and F_{y2} are the components of the radial force generated by the magnetic bearing 2 along x_2 and y_2-axis directions; F_{mx1}, F_{my1}, F_{mx2} and F_{my2} are the components of the external disturbance generated by the motor due to the eccentric shaft displacement along x_1, y_1, x_2 and y_2-axis directions, respectively; d_{x1}, d_{y1}, d_{x2} and d_{y2} are the components of the disturbance generated by the axial motion of the shaft along x_1, y_1, x_2 and y_2-axis directions, respectively.

The mechanical model given by (6) represents four SISO decoupled systems. This equation allows a preliminary study of the system behavior for various types of controllers and parameters of the model. Figure 8 shows the Matlab-Simulink simulation model.

A lead-lag position controller has been designed for each direction using the linear system theory. The transfer function corresponding to the *y*-axis is given by

$$G_{cy}(s) = \frac{2.7\times10^{6}(s+60)(s+20)^{2}}{s^{2}(s+300)}. \qquad (7)$$

The presence of integrators is necessary to obtain null steady-state error for step inputs at reference (as in the case of levitation starting) and step or ramp disturbances at the plant input.

During system operation the main disturbance occurs as a consequence of axial motion. Figure 9 shows the signal d_{y1}. The transient response corresponding to the y_1-axis motion is shown in figure 10. It can be seen that the AMB has a fine dynamic performance since the maximum magnitude of y_1 is quite small.

CONCLUSIONS

A DC-excited primitive bearingless machine used as an AMB for a TLIM shaft was proposed in this paper. Simulation results showed that a stable magnetic suspension can be accomplished with the proposed controller.

Results of the FEA suggest that the AMB actuator is qualified to levitate the secondary of the TLIM.

The relationship between the radial force and the suspension winding current is linear with a small eccentric shaft displacement and it depends on the torque and suspension winding currents beyond of the derivative mutual inductance. This derivative of the mutual inductance can be estimated by FEA.

The worst case in terms of operation conditions was considered in the analysis. When operating in the real world the system will be installed either at the vertical position or with small inclination with respect to the horizontal, which are both more favorable situations.

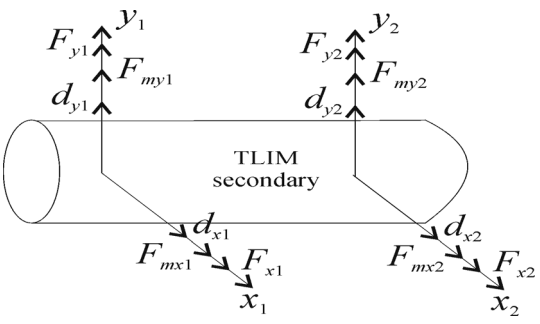

FIGURE 7: Scheme of forces acting on the shaft.

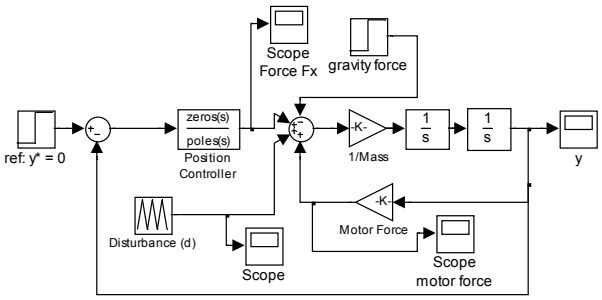

FIGURE 8: Matlab-Simulink model of the control system.

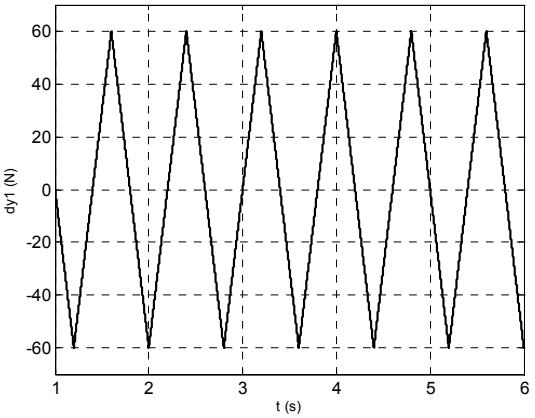

FIGURE 9: Input disturbance d_{y1}.

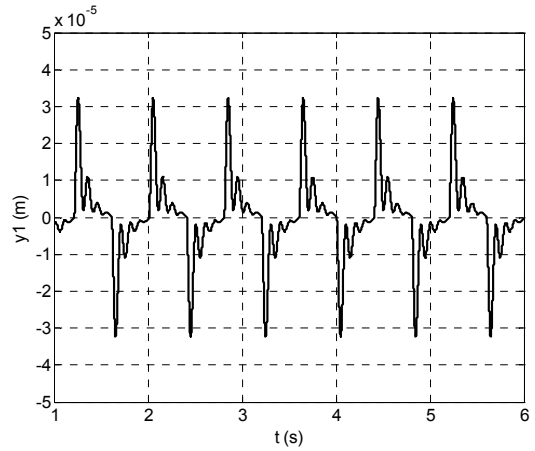

FIGURE 10: Transient response along the y_1-axis due to the disturbance d_{y1}.

REFERENCES

[1] B. P. Alvarenga, "A proposal of application of a tubular linear induction motor for oil extraction", PhD. Thesis, EPUSP, Brazil, 2004 *(in Portuguese)*.

[2] B. P. Alvarenga, I. E. Chabu, J. R. Cardoso. “Thermal Characterization of Long Electrical Devices – Application to a Tubular Linear Induction Motor”, *Proceedings of the IEEE-IEMDC*, 2003, vol.2, pp.938-942.

[3] W. M. Rossini, B. P. Alvarenga, I. E. Chabu, J. J. Cruz, J. R. Cardoso, R. M. Sales, “A new conception for subterranean oil pumping” *I Petroleum and Chemical Industry Conference, IEEE-PCIC*, Brazil, 2006, vol.1, pp. 82-91 *(in Portuguese*).

[4] M.E.F. Kasarda, “An Overview of Active Magnetic Bearing Technology and Applications” *The Shock and Vibration Digest, 2000, pp. 91-99.*

[5] G. Schweitzer, H. Bleuler and A. Traxler, *Active Magnetic Bearings: Basics, Properties and Applications of Active Magnetic Bearings.* Authors Reprint, Zürich, 2003.

[6] A. Chiba, T. Fukao, O. Ichikawa, M. Oshima, M. Takemoto and D.G. Dorrell, *Magnetic Bearings and Bearingless Drives.* Boston: Elsevier Newnes Press, 2005.

[7] A. Chiba, D. T. Power and M. A. Rahman, “Characteristics of a bearingless induction motor” *IEE Transactions on Magnetics*, vol.27, no. 6, pp. 82-91, Nov, 1991.